Partial discharge detection on power equipment using a magneto-resistive sensor

Chen, Yun; Castro Heredia, Luis Carlos; Smit, Johan J.; Ghaffarian Niasar, Mohamad; Ross, Robert

DOI
10.1016/j.ijepes.2023.109270

Publication date
2023

Document Version
Final published version

Published in
International Journal of Electrical Power & Energy Systems

Electrical Power and Energy Systems 152 (2023) 109270

Contents lists available at ScienceDirect

International Journal of Electrical Power and Energy Systems

journal homepage: www.elsevier.com/locate/ijepes

Partial discharge detection on power equipment using a magneto-resistive sensor☆

Yun Chen [a,c,1,*], Luis Carlos Castro Heredia [a], Johan J. Smit [a,b], Mohamad Ghaffarian Niasar [a], Robert Ross [a,b]

[a] High Voltage Technologies Group, Faculty of Electrical Engineering, Mathematics & Computer Science, Delft University of Technology, Delft 2628 CD, The Netherlands
[b] IWO, Institute for Science and Development, Ede 6711 GG, The Netherlands
[c] School of Electric Power Engineering, South China University of Technology, Guangzhou 510640, People's Republic of China

ARTICLE INFO

Keywords:
Cross-linked polyethylene (XLPE) cable
(Electro)magnetic field measurement
Giant magneto-resistive (GMR)
Gas-insulated systems (GIS)
High-frequency current transformers (HFCT)
Partial discharges (PD)
Sensors

ABSTRACT

Partial discharges (PD) detection is an effective diagnostic method to assess the insulation condition of electrical power equipment in the high-voltage laboratory or field tests. This paper presents a non-contacting PD detection method for power equipment. The method is based on an extra high-sensitivity adapted giant magneto-resistive (xMR) sensor that measures the magnetic field produced by the PD currents. Firstly, this paper describes the sensor's relevant principle and signal conditioning circuit. Next, the sensor's typical performance, including the frequency response and time-domain response to calibrator PD pulses, is measured and compared with our previous work. The results indicate that the xMR system's bandwidth is improved to the MHz range. Finally, PD experiments are carried out and compared with measurements using a commercially available high-frequency current transformer (HFCT), which allows for verification of the coherence of the results concerning the PD pulses and phase-resolved PD (PRPD) patterns. The results show that PD in a cross-linked polyethylene (XLPE) cable or a gas-insulated system (GIS) with artificial discharging defects is successfully measured, demonstrating the sensitivity and performance of the xMR system for PD detection.

1. Introduction

Cross-linked polyethylene (XLPE) underground cables and gas-insulated systems (GIS) are vital parts of transmission and distribution power grids [1–2]. It is well known that condition monitoring is important to guard any power equipment's reliability and save maintenance costs. Failures in equipment mainly come from insulation failures. An important indicator of discharge-related imminent insulation failures is the occurrence of partial discharges (PD) [3–4]. In power cables, PD occurs at insulation defects, particularly in cable joints and terminations, especially at material interfaces [5]. In GIS, defects such as undesired metal particles approaching the conductor and triggering a flashover, or lying on a spacer and leading to carbonization, will cause intense electric fields that can create PD [6]. Therefore, PD detection plays a key role in the diagnostic tests of high-voltage equipment to detect defects in the dielectric system.

Regarding PD detection on power cables, high-frequency current transformers (HFCT) are most commonly applied, with the advantages of almost non-invasive installation. However, the HFCT has to be clamped around the ground connection of the system to be tested, leading to issues regarding installation, convenience and insulation interference. Besides, since PD measurements with HFCT are most often carried out at the cable termination, PD pulses from the joints propagate through the cable and suffer from attenuation because joints are underground and remote from the measuring point. Thus, localization is often unavailable or requires two or more HFCTs to realize time-domain reflectometer (TDR) analysis [7–10]. On the other hand, PD detection in GIS is commonly performed using the UHF method. Nevertheless, the

☆ This work was supported by the EU H2020 R&I program and the Ministry of Economic Affairs and Climate, Netherlands, under ECSEL Grant agreement No 876659 (iRel4.0).

* Corresponding author.
E-mail addresses: Y.Chen-17@tudelft.nl, epchenyun@mail.scut.edu.cn (Y. Chen), L.C.CastroHeredia@tudelft.nl (L.C.C. Heredia), J.J.Smit@tudelft.nl (J.J. Smit), M.GhaffarianNiasar@tudelft.nl (M.G. Niasar), Rob.Ross@tudelft.nl (R. Ross).

[1] Supported by the China Scholarship Council (CSC) under Grant 202106150039, and now with the High Voltage Technologies Group, Faculty of Electrical Engineering, Mathematics & Computer Science, Delft University of Technology, Delft, 2628 CD, the Netherlands.

https://doi.org/10.1016/j.ijepes.2023.109270
Received 20 January 2023; Received in revised form 13 April 2023; Accepted 21 May 2023
Available online 31 May 2023

pulsed signals, for instance, PD signals or transients.

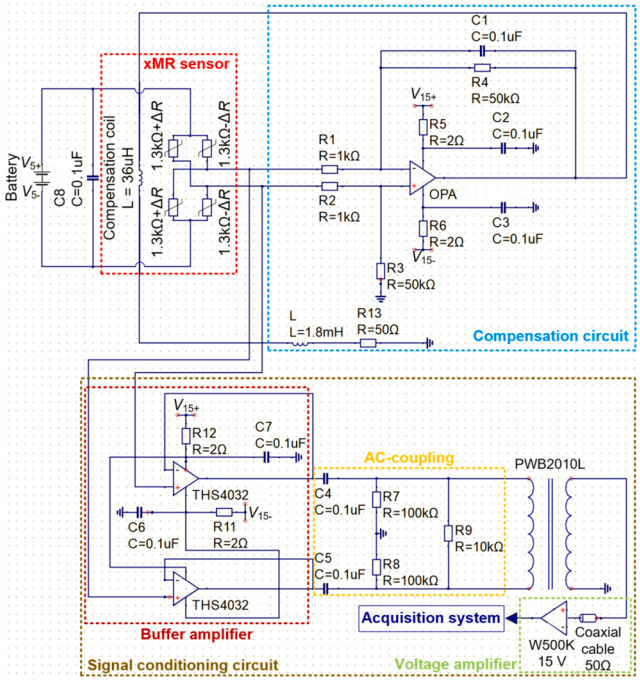

Fig. 1. Schematic diagram of the xMR system.

Fig. 1. Schematic diagram of the xMR system.

electromagnetic waves in GIS structures suffer from attenuation and distortion, mainly in the higher-order modes [11–12].

Based on the above analysis, the existing PD detection methods are very useful. However, they have limitations of intrusive access to the device, e.g., connecting to a circuit in series, facing issues regarding convenience, insulation, and additional interference. Therefore, non-invasive measurement techniques for power equipment are needed, focusing on contactless measurements with highly sensitive sensors to avoid the abovementioned problems.

With the rapid development of magnetic electronic devices, magneto-resistive sensors are increasingly finding applications for contactless detection of electric currents both in low and high-power electric systems. For example, Tsinghua University designed a giant magneto-resistive (GMR) current sensor to monitor steady-state and transient currents in the power grid [13]. Similar studies have been reported by Transilvania University of Brasov, which implemented a differential GMR system for DC/AC current measurement [14]. Due to their performance limitations, they are usually designed and employed only for detecting DC and low-frequency currents. On the other hand, the application of GMR technology has not been limited to low-frequency applications. Beihang University used a GMR sensor to detect fast transient signals from a PD calibrator with different discharge quantities and repetition rates. The minimum discharge quantity detected is 50 pC [15]. Similarly, Tsinghua University proposed using a dual-axial TMR sensor device for corona discharge location, which was easier to use than the standard probes [16]. However, these studies mainly focus on laboratory studies with small test objects like calibrator or PD model defects' signals, no attempts have been reported aiming at this sensor's application on actual cables or GIS.

Our contribution [17] also performed PD experiments based on GMR technology on corona and surface models. It designed compensation and signal conditioning circuits (referred to as Circuit 1) for an extra high-sensitivity adapted giant magneto-resistive (xMR) sensor for non-contacting PD detection. The results prove that PD can be detected and evaluated by this technology. However, bandwidth and sensitivity limitations still make it challenging to use such an xMR system to detect PD signals on actual power equipment.

The present work describes a non-contacting PD detection method that employs an xMR sensor with a signal conditioning circuit (referred to as Circuit 2) integrated with a higher bandwidth component to achieve better bandwidth and sensitivity. The frequency response and time-domain response to fast calibrator pulses by the xMR sensor with Circuits 1 and 2 are compared to verify its bandwidth performance. The xMR sensor with Circuit 2 is evaluated in high-voltage experiments on a XLPE cable and a GIS with artificial discharging defects. The ability of this approach for PD detection and further application are also discussed.

2. GMR-based non-contacting sensing technology

The GMR-based PD sensing technology will be discussed in the three following subsections. First, the principle of the GMR sensor is presented, followed by a description of the xMR system. Likewise, the experimental characterization of the frequency and time-domain responses of our xMR system for PD detection is shown.

2.1. Principle of GMR sensor

The GMR effect is a significant change in the resistance in multi-layered structures due to the relative orientation of the magnetization vectors. For practical application, a GMR sensor is usually connected in a bridge configuration with four resistive elements, as shown in Fig. 1. Under an external magnetic field, the bridge is unbalanced due to the variation in the sensor resistance ($\pm\Delta R$), which results in the bridge output voltage.

2.2. The xMR system

The schematic diagram of the xMR system is shown in Fig. 1. The xMR sensor is powered by a constant current from a battery and connected to a compensation circuit. A compensation coil of ~ 36 μH is positioned at the xMR sensor and connected in a closed-loop current configuration to compensate external magnetic fields, improve linearity, reduce hysteresis, and reduce temperature drift [18]. The compensation of the external magnetic fields is effective from DC to a cut-off frequency of $f_{cut} = 36$ kHz. The output of the xMR sensor in this frequency band is fed to a low-offset, precision amplifier OPA that drives the necessary current into the compensation coil. Although the unity-gain of the OPA is 2.5 MHz, C1 and L in the compensation circuit add extra poles to the closed-loop gain. As a result, above f_{cut}, the circuit gain is < 0 dB rendering the compensation almost negligible, and the xMR sensor can be used to selectively react to the magnetic field created by fast pulsed signals, for instance, PD signals or transients.

In turn, the xMR sensor's output is taken to the signal conditioning circuit. In our previous work, the xMR sensor output is amplified by an instrumentation amplifier (Analog Devices, AD8429) with a unity-gain at 15 MHz. Although the instrumentation amplifier proved to be a good solution, because of its high common-mode rejection ratio and high input impedance, there are still limitations to reaching broader bandwidths with the instrumentation amplifiers commercially available. Thus, one solution to have a broad bandwidth and still a high common-mode rejection ratio is to adopt a differential to single-ended stage before the signal amplification. This paper uses a radio frequency (RF) transformer (Coilcraft, PWB2010L) with a bandwidth of 0.0035 ~ 125 MHz as a balun. At low frequencies, the impedance of the RF transformer is very low compared to the xMR bridge, then the RF transformer loads the bridge affecting its response, therefore, a buffer amplifier (Texas Instruments, THS4032) is used as a decoupling impedance stage. The AC-coupling stage before the RF transformer is used to avoid the loading and clipping of the buffer amplifier at low frequencies where the RF transformer is a low impedance.

Besides, to improve the transient response of the xMR, a 100 nF capacitor C8 in Fig. 1 has been added in parallel to the voltage supply of

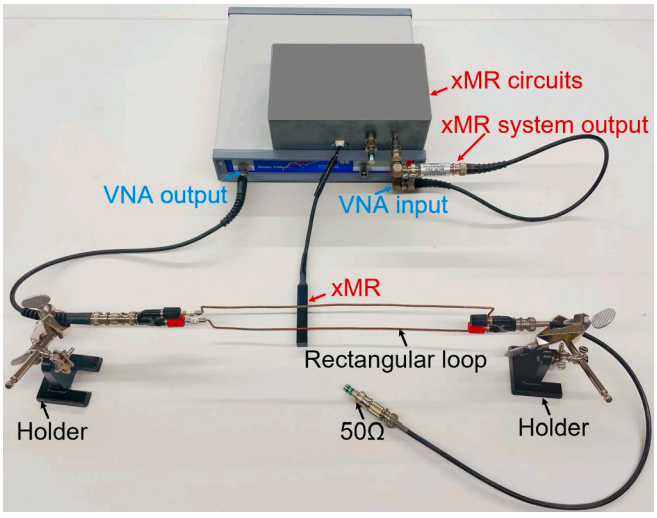

Fig. 2. The frequency response measurement set-up of the xMR system.

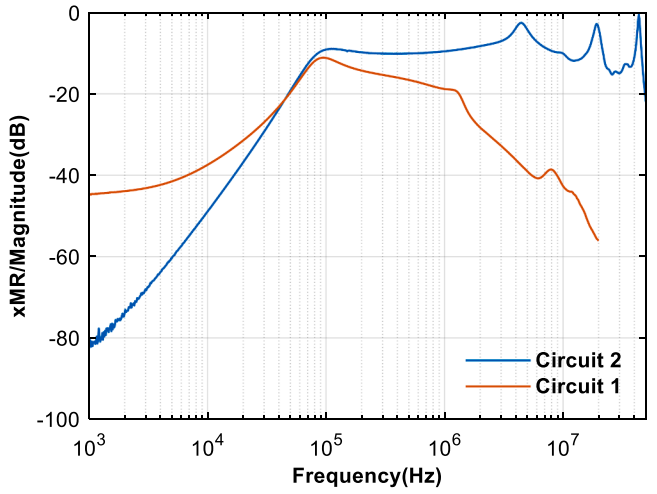

Fig. 3. Frequency response of the xMR system with Circuits 1 and 2 (at same source level 225 mVrms).

the xMR. C8 supplies the transient current drawn by the change in the xMR bridge.

Finally, a voltage amplifier (Tron-Tech, W500K 15 V) with a gain of 34 dB is added to the output of the RF transformer to step up the xMR system's sensitivity.

2.3. Frequency response of the xMR system

A rectangular loop is used to characterize the performance of the xMR system. The rectangular loop, shown in Fig. 2, has two BNC connectors at each end.

Frequency response measurements of the xMR system are conducted using a Vector Network Analyzer (VNA, Omicron Lab, Bode 100). Before conducting the frequency response measurements of the xMR system, a calibration is performed to ensure that the measurement set-up (loop, cables, wires, BNC connectors, etc.) itself has no resonances and does not influence the actual measurements. After calibration, the interferences of the measurement set-up are compensated so that the actual response of the xMR system can be measured.

The VNA sweeps from 10 kHz ~ 50 MHz with a source level of 0 dBm (225 mVrms) in one BNC of the rectangular loop while the other is terminated with a 50 Ω resistor.

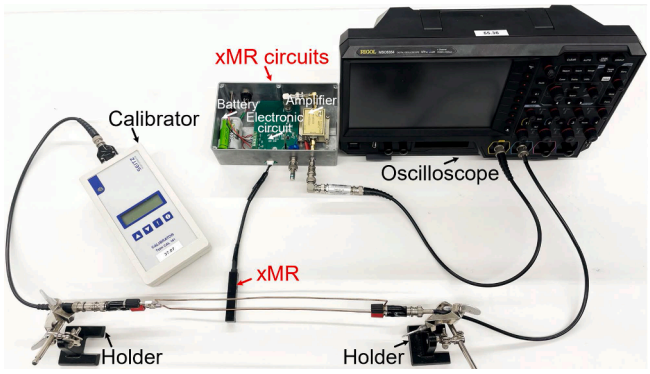

Fig. 4. Measurement set-up for the response of the xMR system to calibrator pulses.

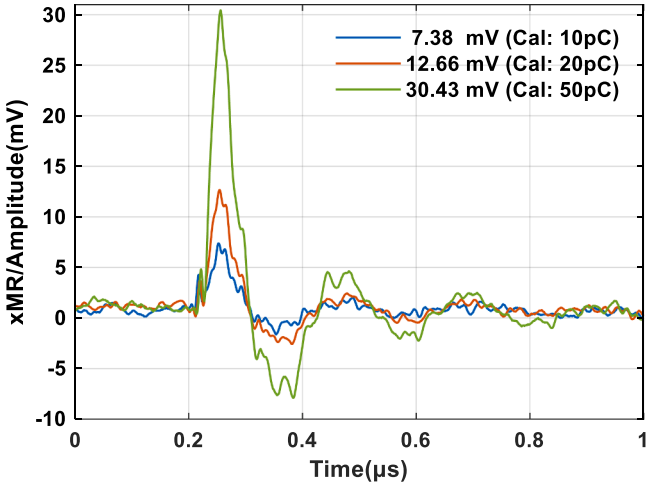

Fig. 5. Xmr system's responses to calibrator pulses of different charges.

The sensitivity axis of the xMR sensor is positioned perpendicular to the loop plane, around 6 mm from the loop wire carrying a current of 225 mVrms/50 Ω = 4.5 mArms. The xMR system response is then measured at the output of the voltage amplifier.

Fig. 3 compares the frequency response of the xMR system with Circuits 1 and 2. It can be seen that the very low-frequency signals are attenuated due to the closed-loop compensation circuit that brings the xMR bridge output close to zero, while the high-frequency signals created by PD events or transients go through reaching the output voltage amplifier. The xMR system's high-frequency response with Circuit 2 levels off with a small rise to a narrow peak at 4.44 MHz. At higher frequencies, other resonance peaks appear at 19.14 MHz and 43.68 MHz. Conversely, with Circuit 1, the frequency response decreases continuously right after the peak of around 100 kHz.

2.4. Time-domain response of the xMR system

Time-domain response measurements of the xMR system are carried out using a standard PD pulse calibrator (Seitz Instruments, CAL 141) to check the xMR system's sensitivity to fast pulses, as shown in Fig. 4.

The calibrator injects signals with charges of 10/20/50 pC in one BNC of the same rectangular loop while the other is connected to an oscilloscope (Rigol, MSO5354) with 50 Ω input impedance.

The time-domain response of the xMR system to the calibrator pulses is shown in Fig. 5. The xMR system output is a pulsed signal with oscillations due to some small high-frequency peaks in the frequency response in Fig. 3.

Besides, the xMR system's responses to calibrator pulses of 50 pC

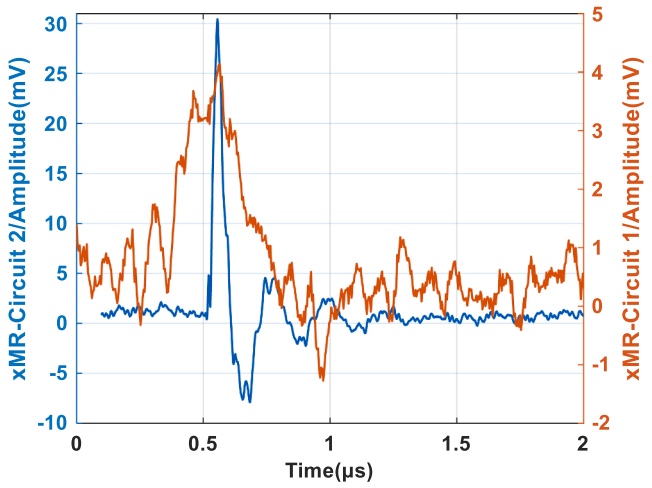

Fig. 6. Comparison of the xMR system's responses to calibrator pulses of 50 pC charges with Circuits 1 and 2.

Table 1
Comparison of the xMR System's Responses to Calibrator Pulses with Circuits 1 and 2.

xMR system	Parameters	
	Ratio	Minimum detectable charge (pC)
Circuit 2	14.35	10
Circuit 1	3.16	50

charges with Circuits 1 and 2 are compared in Fig. 6 and Table 1. The ratio (peak signal amplitude/background noise) of the xMR system with Circuit 2 has improved by around 4.5 times. Moreover, the minimum detectable charge for the xMR system is 10 pC compared with Circuit 1, which can only detect as low as 50 pC. This confirms that the xMR system with Circuit 2 has better bandwidth and sensitivity.

3. PD experiment

PD experiments in this paper aim to evaluate the response and performance of the xMR system to actual PD signals from a power cable and a GIS.

3.1. PD experimental set-up for XLPE cable

A 6/10 kV XLPE cable system with an artificial internal defect to create PD activity has been used for the PD experiments. Although the xMR system was proved to be able to detect PD signals from cable defects [17], in this contribution, the experimental set-up has been extended to reproduce the actual operating condition of the test cable and its effects on the compensation circuit of the xMR system. Thus, apart from the conventional high-voltage transformer and its necessary control and instrumentation, a current transformer has been added to induce a current ranging from 100 ~ 200 A in the cable. Particularly, two sections of cable, 3 m and 6 m in length, are connected, forming the secondary winding of the current transformer. The physical layout of the experimental set-up can be seen in Fig. 7a.

In the 3 m long cable, a plastic tie-wrap strip has been inserted at the interface between the cable XLPE insulation and the cable joint's inner semi-conductive layer to produce internal PD is indicated in Fig. 7b and Fig. 7c.

The xMR system is placed close to and in parallel with the axial direction of the cable but with different positions; details will be mentioned in subsequent sections. In both cases, the xMR sensor is in the close vicinity of the intense 50 Hz magnetic field of the current flowing

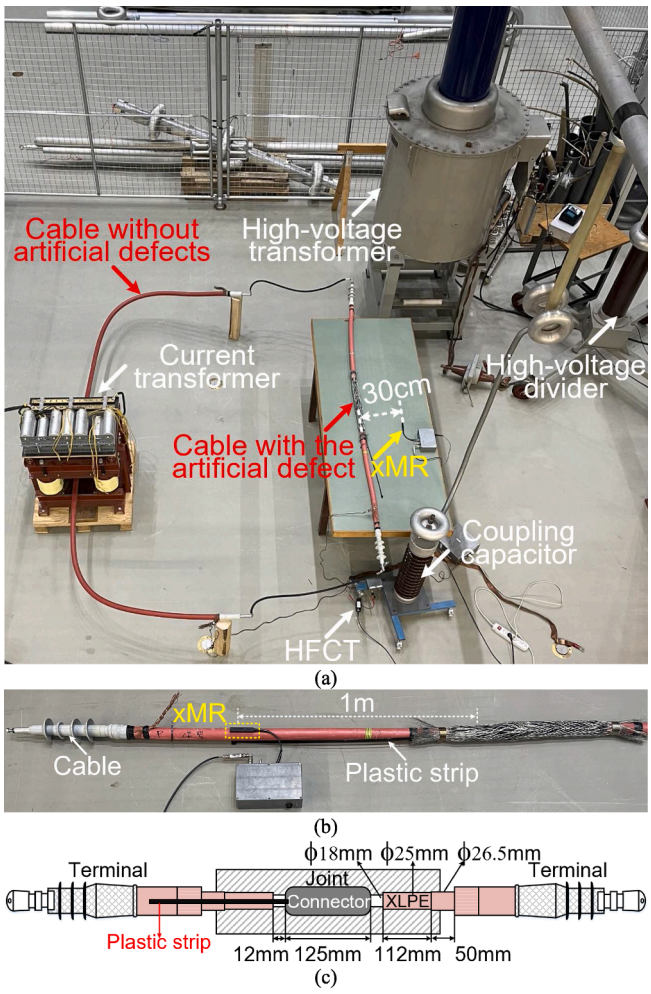

Fig. 7. PD experimental set-up for the 6/10 kV XLPE cable system. (a) Laboratory arrangement, (b) The XLPE cable with the artificial internal defect, (c) Schematic diagram of the XLPE cable with the artificial defect.

in the cable. Therefore, the experiments aimed at testing the effectiveness of the compensation circuit to avoid the saturation of the xMR bridge.

It is also important to mention that the xMR system validation is done using a known PD reference signal. Thus, this set-up also includes a coupling capacitor connected in parallel with the cable to provide a low-impedance and high-frequency path for the PD signals. An HFCT (Techimp, HFCT30) with a bandwidth of 1 ~ 50 MHz is mounted on the ground side of the coupling capacitor and provides the PD reference signal.

3.2. PD experimental set-up for GIS

In GIS systems, PD signals travel along the main conductor and compartments, similar to traveling waves in a coaxial structure. In the vast majority of in-service GIS, the spacers in between individual compartments introduce gaps in the enclosure of the GIS allowing part of the electromagnetic energy of the PD signal to leak out of the compartments.

Therefore, a full-size 380 kVac GIS with multiple spacers, a ground switch, a circuit breaker, a T-joint connection, and an L-branch structure [19] serves as a test object for our xMR system, as shown in Fig. 8a.

For this experiment, a test cell is used to produce free-moving particle discharges and is installed at one end of the GIS, as shown in Fig. 8b. The particle is an aluminum curly-shaped ball with a diameter of around 0.5 cm. In the experiments, the xMR is located at the second spacer, 2.5

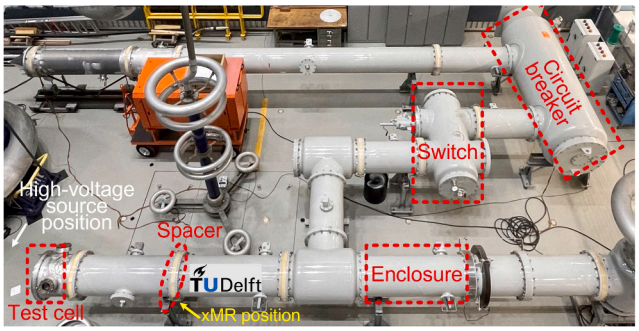

(a)

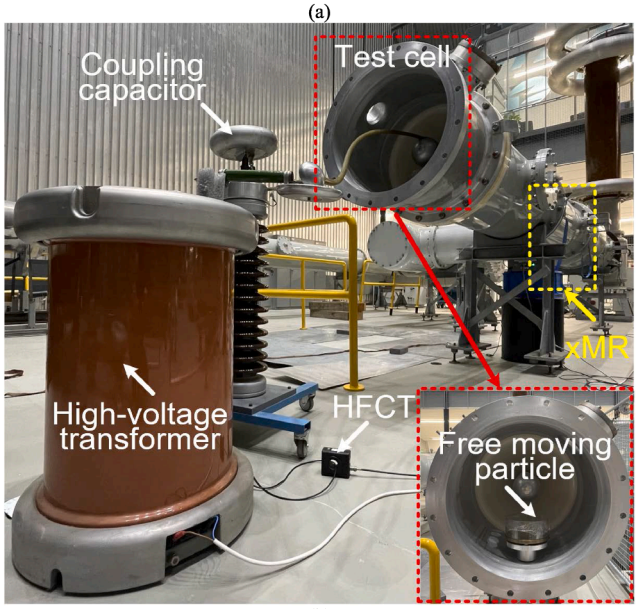

(b)

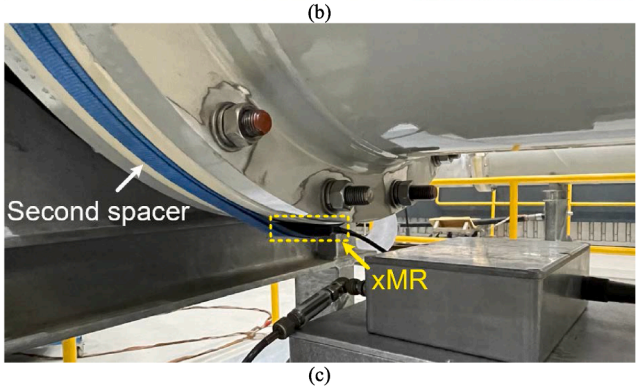

(c)

Fig. 8. PD experimental set-up for the GIS. (a) GIS layout, (b) PD experimental set-up, (c) Position of the xMR system.

m from the test cell, as shown in Fig. 8c. Likewise, a coupling capacitor and an HFCT are installed next to the test cell to be used as a reference.

4. Experimental results and discussions

In this section, a collection of PD experimental results, including the phase-resolved PD (PRPD) patterns and PD pulses of the cable and the GIS, are reported to verify the sensitivity and performance of the xMR system.

4.1. PD reference signal

The PD level produced by the defect in the cable joint is measured by a conventional PD detector (Techimp, PDBase II) based on the standard

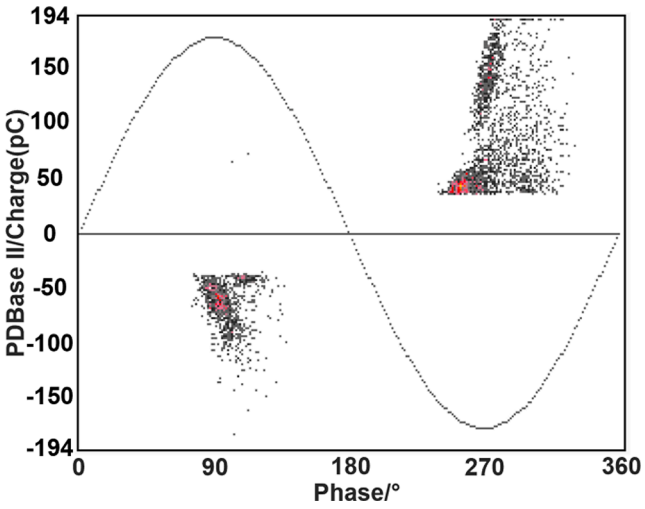

Fig. 9. The PRPD pattern from the cable joint with the artificially created PD defect measured by a conventional PD detector.

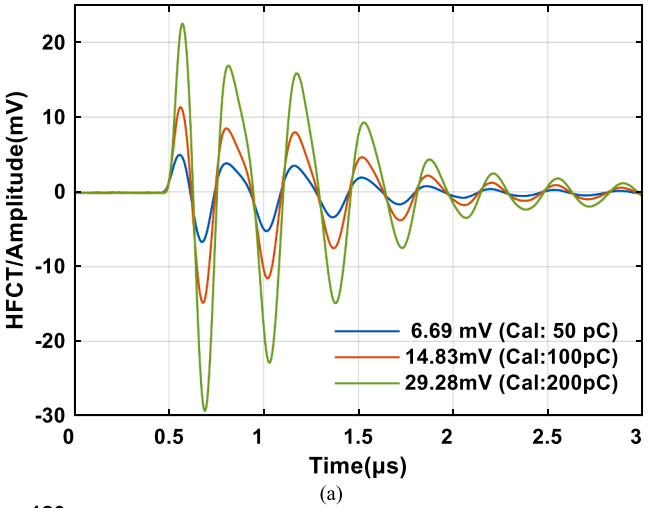

(a)

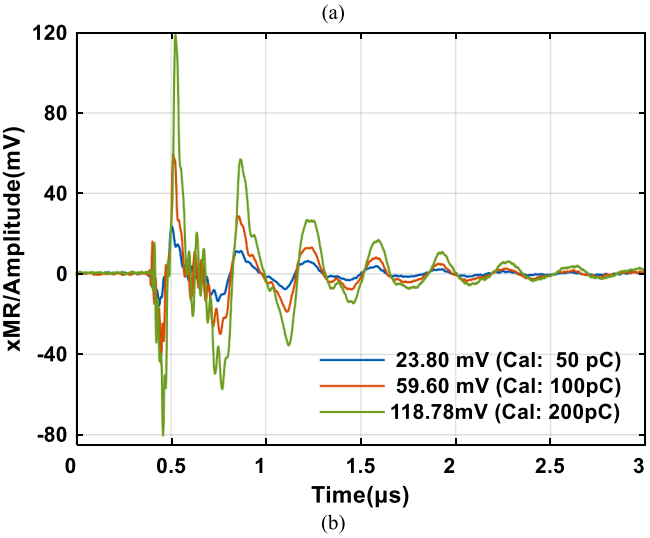

(b)

Fig. 10. Test circuit response to calibration signals. (a) HFCT, (b) xMR system.

IEC 60270, as shown in Fig. 9. This is needed for two purposes. First, we aimed to control the PD level in a few tens of pC levels which is comparable to what can occur in cables in service. According to the PRPD pattern from the PDBase II in Fig. 9, the PD level with the highest

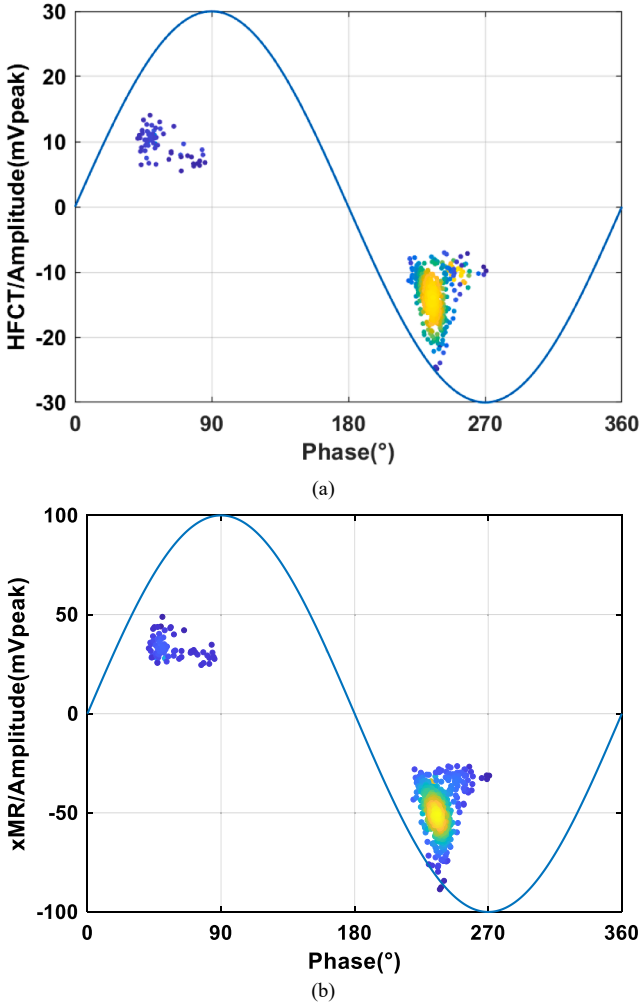

Fig. 11. The PRPD patterns from the cable defect when the xMR sensor is 1 m away from the defect and on the cable outer mechanical sheath. (a) HFCT, (b) xMR system.

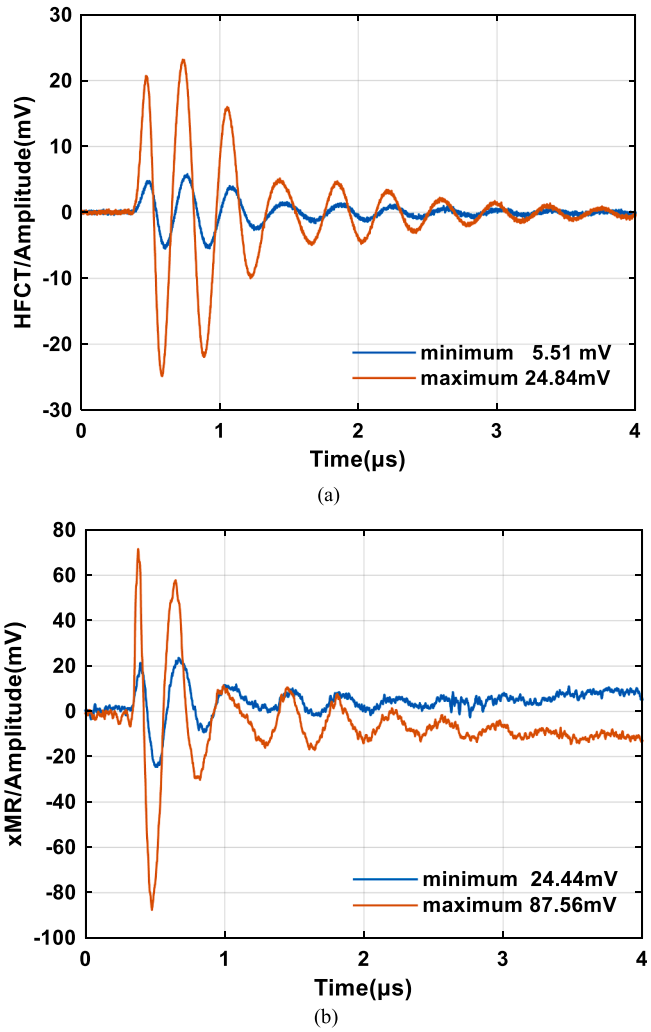

Fig. 12. The maximum and minimum PD pulses of the cable when the xMR sensor is 1 m away from the defect and on the cable outer mechanical sheath. (a) HFCT, (b) xMR system.

repetition rate is around 50 pC.

Secondly, the wideband acquisition of calibrator signals allowed us to know the time-domain response of the whole test circuit. Thus, calibration signals ranging from 50 ~ 200 pC are injected into the test cable, and the outputs of the HFCT and xMR system are measured using an oscilloscope (Tektronix, MSO 58B).

The measured waveforms, as depicted in Fig. 10, show a resonance peak around ~ 3 MHz due to the strong LC characteristic of the whole test circuit. This resonance peak falls within the bandwidth of both sensors, i.e., HFCT and xMR system, so their outputs both show the same oscillating behavior. Furthermore, this peak happens at such a low frequency that even actual PD signals will excite the same oscillating response. This, in fact, is used in this paper as a way to validate that the xMR system's output corresponds to actual PD signals. In other words, all the acquisitions are checked for the frequency peak at ~ 3 MHz. If it is present both in the HFCT and xMR system's output, then the acquisition is considered a valid PD acquisition.

4.2. PD results of XLPE cable

With a current of 200 A flowing in the high-voltage cable loop, the xMR sensor is placed 1 m away from the PD defect and on the cable outer mechanical sheath, and a test voltage of 9.1 kVrms is applied to the cable.

In all measurements, the xMR system and HFCT outputs are recorded simultaneously using the xMR signal as the trigger of the oscilloscope. Because the xMR system and HFCT outputs are acquired simultaneously, they are expected to produce identical in-phase patterns. This can be verified in Fig. 11, where in addition, the shape of the pattern conformed to the typical pattern created by internal discharges.

Moreover, the amplitude of the pattern from the xMR system follows closely that from the HFCT, thus, further validating that the xMR system is indeed reacting to PD signals.

As a final validation, all the waveforms from the xMR system and HFCT are inspected for the presence of the oscillating frequency around 3 MHz with the help of the software tool PDflex [20].

The acquired waveforms with maximum and minimum amplitudes from the HFCT and the xMR system, corresponding to the same trigger event, are compared, as shown in Fig. 12. The maximum and minimum amplitudes from the xMR system are 87.56 mV and 24.44 mV, respectively.

In the second set of measurements, aiming at verifying the overall sensitivity of the xMR system, the xMR sensor is placed parallel to the axial direction of the cable but 30 cm away from its outer sheath, as shown in Fig. 7a.

The PRPD patterns obtained from the HFCT and the xMR system are shown in Fig. 13. The pattern phase characteristic verifies that the acquisition is correct and the xMR system is still properly picking up the magnetic field produced by the PD pulses even at a 30 cm distance from

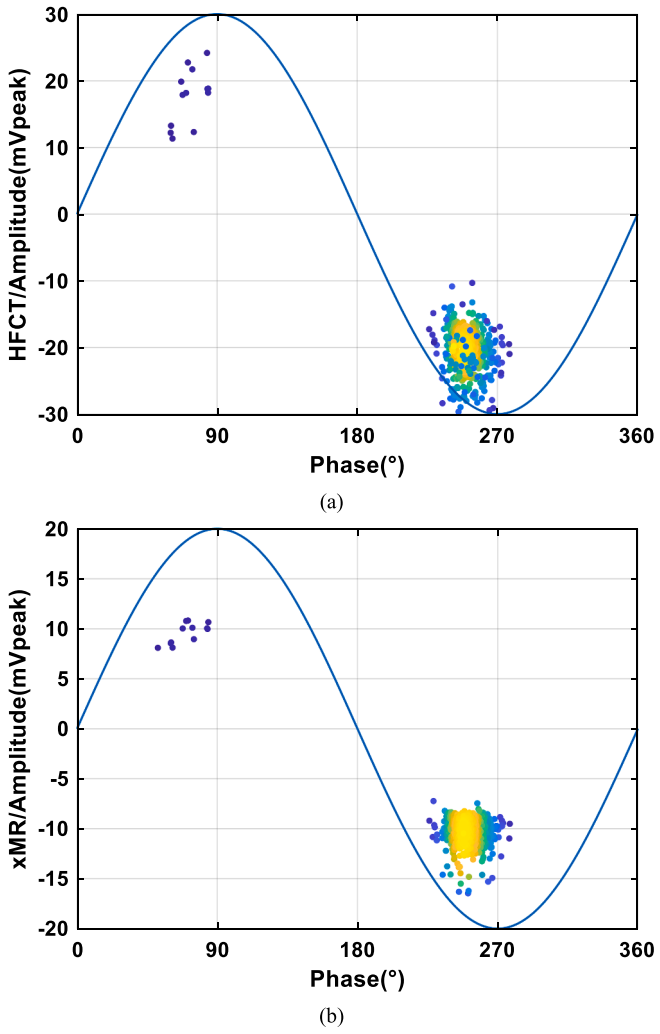

Fig. 13. The PRPD patterns from the cable defect when the xMR sensor is 30 cm away from the cable outer sheath. (a) HFCT, (b) xMR system.

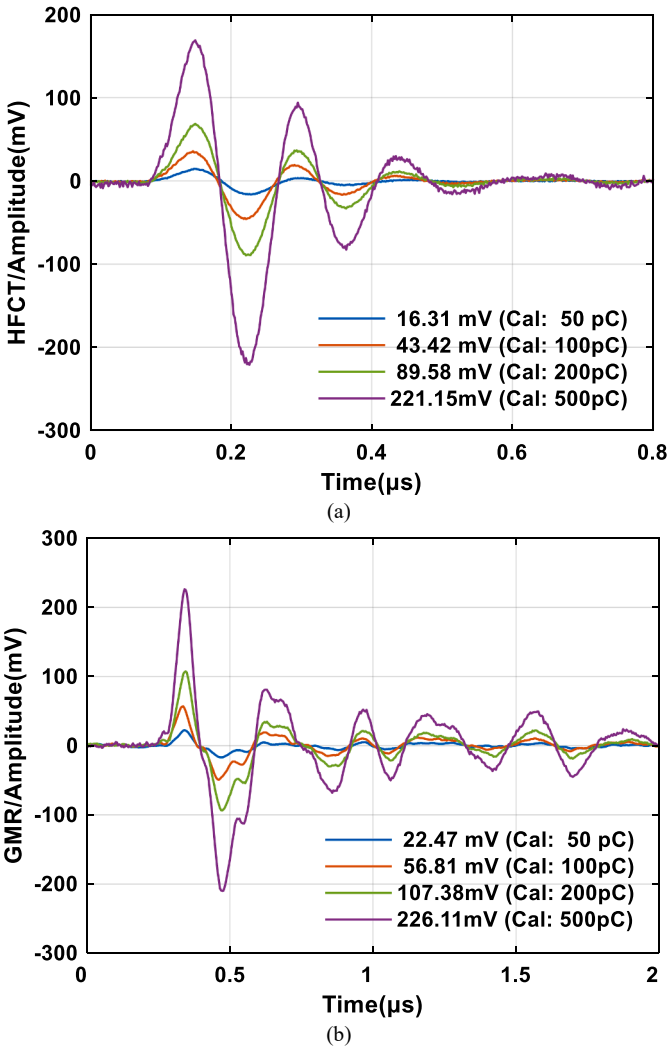

Fig. 14. Measurement results with injected signals of different charges from the pulse calibrator for the GIS. (a) HFCT, (b) xMR system.

the cable. The reduced sensitivity of the xMR system with distance led to the loss of most of the positive parts of the pattern from Fig. 11b, and only the largest part of the negative part is recorded.

4.3. PD results of GIS

First, measurement results with injected signals of different charges from the pulse calibrator for the GIS are shown in Fig. 14.

In a GIS system, PD radiates electromagnetic waves in a frequency spectrum ranging from DC to GHz. These electromagnetic waves induce surface currents in the main conductor and the external enclosure. The homogenously distributed surface currents flow along the compartments, the electrical paths in the spacers, the L branches, T joints, or any other electrical paths in the GIS. The detection of the PD signals is achieved via the xMR system by measuring the surface currents created by the PD. [11,19,21].

Then, PD experiments are performed on the GIS at a voltage of 59 kVrms. The PRPD patterns obtained from the HFCT and the xMR system are depicted in Fig. 15, using the HFCT signal as the trigger source, which show no significant differences.

A free-moving particle in contact with the enclosure of an energized GIS acquires an induced surface charge whose interaction with the background electric field exerts a Coulomb force on the particle itself. The particle lifts off as soon as the Coulomb force exceeds the gravitational force, after which it is accelerated towards the electrode. The particle dynamics are governed by the induced net charge deposited on its surface, which is, in turn, dependent on the voltage magnitude at the instant of lift off (background electric field), and the particle shape (distorted electric field). Therefore, a sinusoidal-like trajectory is expected under AC voltage [6].

After that, the PRPD patterns when changing the trigger sources to the xMR signals are shown in Fig. 16. Compared to the PRPD patterns in Fig. 15, the HFCT has almost the same amplitudes of 1 ~ 5 mV, which verifies that the acquisition is correct and that the xMR system is properly acquiring PD signals.

However, notice that the PRPD patterns in Figs. 15 and 16 are slightly different. The magnetic signals are relatively weak when the xMR is far away from the PD source, so the xMR system's sensitivity is reduced, which is why only the top part of the pattern in Fig. 15 can be seen in Fig. 16.

Besides, the detected waveforms with maximum and minimum amplitudes from the HFCT and the xMR system, corresponding to the same trigger event, are compared, as shown in Fig. 17. The maximum and minimum amplitudes from the xMR system are 19.35 mV and 8.68 mV, respectively.

4.4. Discussions

One particular characteristic of the xMR system presented in this

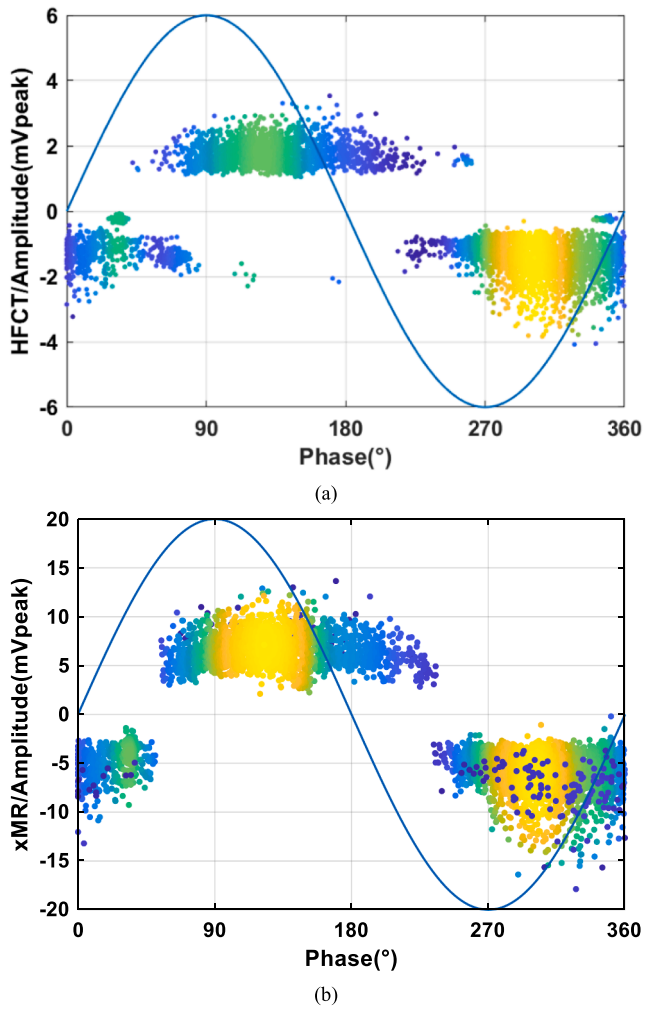

Fig. 15. The PRPD patterns from the GIS defect using the HFCT signal as trigger source. (a) HFCT, (b) xMR system.

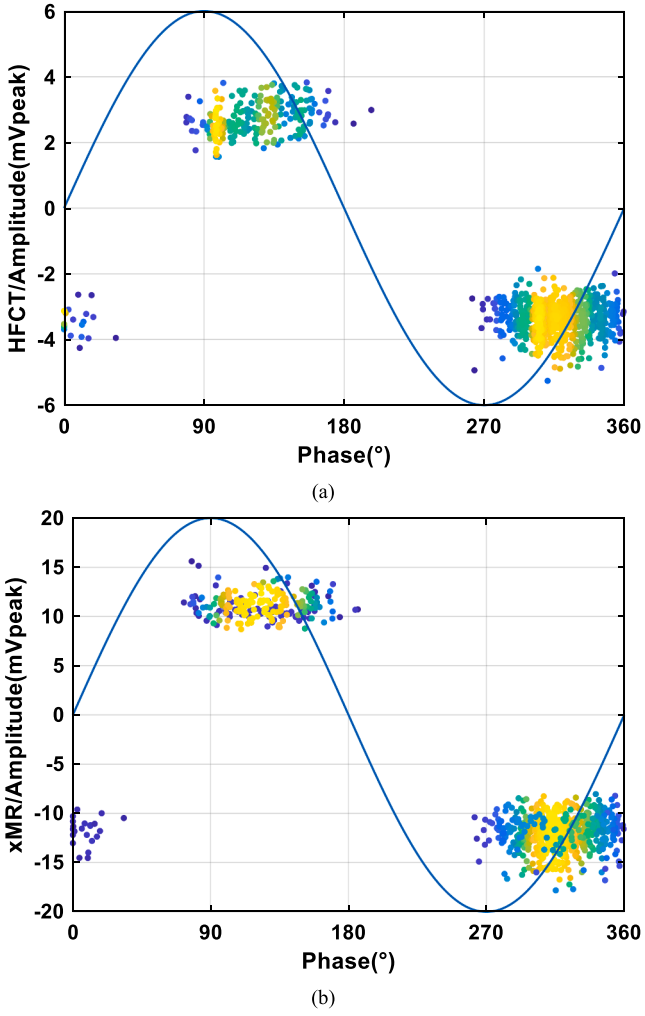

Fig. 16. The PRPD patterns from the GIS defect using the xMR signals as trigger sources. (a) HFCT, (b) xMR system.

paper is its direction sensitivity. In fact, the geomagnetism of ~ 60 μT might be enough to saturate the xMR bridge without the compensation circuit.

Thus, the positioning of the xMR sensor was paramount for the results reported in previous sections. In the case of the high-voltage cable, the current of ~ 200 A created a strong magnetic field higher than the compensation capability of the system; however, the xMR sensor was placed so that the 50 Hz magnetic field vector was perpendicular to the sensitivity axis of the sensor as depicted in Fig. 18. In practice, there is also a 50 Hz component parallel to the sensitivity axis of the sensor, but the experimental results showed that such component was indeed compensated.

On the other hand, one might initially think that the sensor's sensitivity axis is also perpendicular to the magnetic field of a PD pulse that travels along the cable. However, the ground sheath of the cable is made of individual wires wound in a spiral fashion around the cable, as can be seen in Fig. 19. This has two implications. The first one is that the high-voltage cable is not a perfect coaxial structure, and therefore the PD magnetic field leaks out just as in the case of the GIS due to the spacers. The second one is that the transverse orientation of the ground wires allows a significant component of the magnetic field parallel to the sensor's sensitivity axis, thus boosting the sensitivity for PD signals.

5. Conclusion

This paper contributes a system to measure PD signals in a high-voltage cable and from GIS, contactless and based on magnetic field detection using an xMR sensor. A significant improvement o the signal conditioning circuit for the xMR sensor has been reported in this paper as compared to previous contributions from the authors.

From the system point of view, these contributions demonstrated that a low-frequency compensation circuit extends the bandwidth of the xMR bridge to the MHz range enabling its application for PD detection. Even if the compensation capability is limited due to the maximum current of the amplifier OPA driving the compensation circuit, the high direction sensitivity of the xMR sensor can be leveraged to reduce the magnetic field acting parallel to its sensitivity axis and, therefore, to be compensated.

Likewise, the xMR bridge's bandwidth stretch to the MHz range is achieved by using a balun to couple the differential xMR bridge output and a wideband single-ended amplifier. The frequency response results indicate that the xMR system intrinsically has a broad bandwidth mainly limited by the signal condition circuit and parasitics. The GIS measurement results show that the xMR system is indeed sensitive to the high-frequency magnetic fields of the PD signals that leak out via the spacers. On the other hand, the test circuit LC characteristic can create a low-frequency oscillation, as in the case of the experiments with the high-voltage cable. In this particular case, the resonance frequency of ~ 3 MHz falls into the flat band of the xMR system, and therefore its output is easily acquired by the oscilloscope.

The xMR system is also proved to have good spatial sensitivity. The xMR system still detects the PD activities properly, even 30 cm away

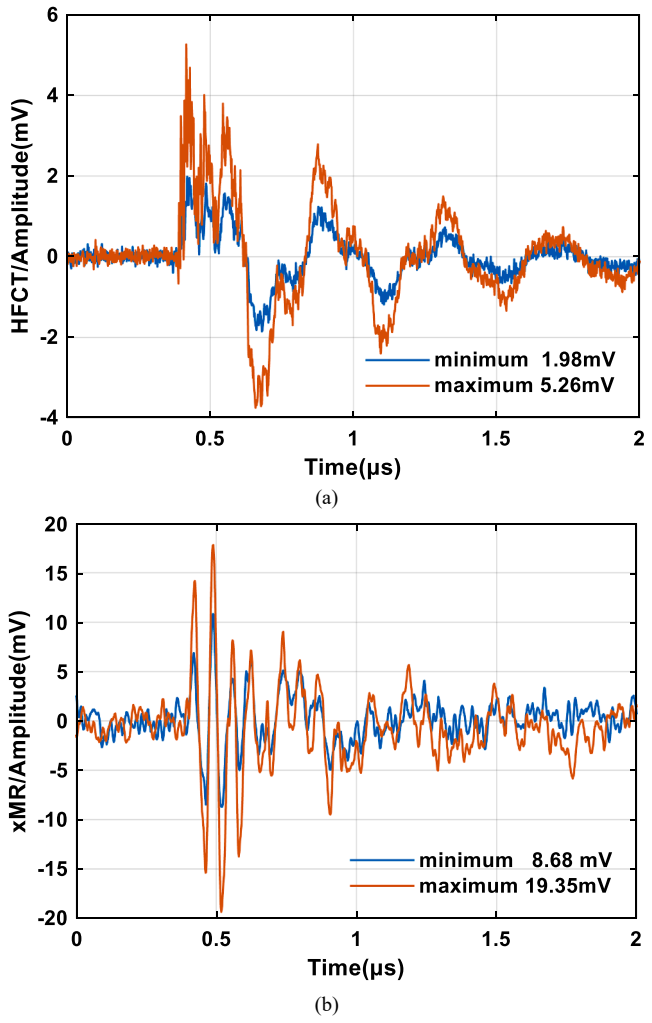

Fig. 17. The maximum and minimum PD pulses of the GIS. (a) HFCT, (b) xMR system.

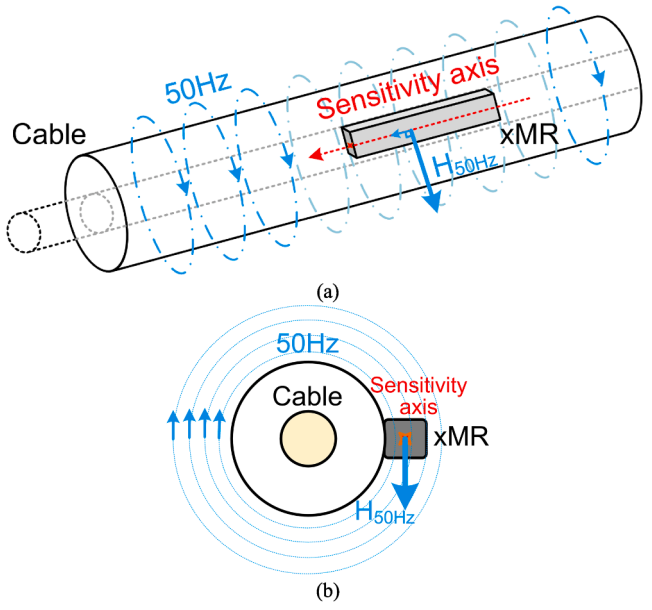

Fig. 18. The positioning of the xMR sensor in the PD experiments. (a) Perspective view, (b) Side view.

Fig. 19. The metal sheath structure of the 6/10 kV XLPE cable.

from the high-voltage cable outer sheath. This makes it possible to use the xMR system as a contactless sensor to probe PD sources at a distance from the power equipment under test, even on powered or inaccessible assets.

CRediT authorship contribution statement

Yun Chen: Methodology, Software, Validation, Formal analysis, Investigation, Data curation, Writing – original draft, Visualization. **Luis Carlos Castro Heredia:** Methodology, Software, Validation, Formal analysis, Investigation, Writing – review & editing, Visualization, Supervision. **Johan J. Smit:** Conceptualization, Resources, Writing – review & editing, Supervision, Project administration, Funding acquisition. **Mohamad Ghaffarian Niasar:** Resources, Writing – review & editing, Supervision. **Robert Ross:** Conceptualization, Resources, Writing – review & editing, Supervision, Project administration, Funding acquisition.

Declaration of Competing Interest

The authors declare that they have no known competing financial interests or personal relationships that could have appeared to influence the work reported in this paper.

Data availability

The data that has been used is confidential.

Acknowledgment

The authors are grateful to Geert Jan Kamphuis, Wim Termorshuizen, and Paul van Nes from the High Voltage Laboratory of the Delft University of Technology for their experimental support in using the high-voltage facilities.

Yun Chen also gratefully acknowledges her supervisors, Academician Licheng Li and Professor Yanpeng Hao at the South China University of Technology, and Professor Mingli Fu at Electric Power Research Institute of China Southern Grid, for their guidance, support, and encouragement.

The authors thank TDK Corporation for supplying the Nivio xMR sensors for this research.

References

[1] Mier C, Mor AR, Vaessen P. Design and characterization of a magnetic loop antenna for partial discharge measurements in gas insulated substations. IEEE Sens J Sep. 2021;21(17):18618–25.
[2] Chen Y, et al. Voltage equivalence of partial discharge tests for XLPE insulation defects. IEEE Trans Dielectr Electr Insul Apr. 2022;29(2):683–92.
[3] Boggs S, Densley J. Fundamentals of partial discharge in the context of field cable testing. IEEE Trans Dielectr Electr Insul 2000;16(5):13–8.
[4] Montanari GC, Cavallini A. Partial discharge diagnostics: from apparatus monitoring to smart grid assessment. IEEE Electr Insul Mag 2013;29(3):8–17.
[5] Wu J, et al. Measuring method for partial discharges in a high voltage cable system subjected to impulse and superimposed voltage under laboratory conditions. Int J Electr Power Energy Syst Feb. 2020;115(105489):1–12.
[6] Piccin R, et al. Partial discharge analysis of gas insulated systems at high voltage AC and DC. IEEE Trans Dielectr Electr Insul Feb. 2015;22(1):218–28.
[7] Stone GC. Partial discharge diagnostics and electrical equipment insulation condition assessment. IEEE Trans Dielectr Electr Insul Oct. 2005;12(5):891–904.
[8] Xu Y, et al. Special requirements of high frequency current transformers in the on-line detection of partial discharges in power cables. IEEE Electr Insul Mag 2016;32(6):8–19.

[9] Montanari GC. Partial discharge detection in medium voltage and high voltage cables: maximum distance for detection, length of cable, and some answers. IEEE Electr Insul Mag 2016;32(5):41–6.
[10] Wu J, et al. Automatic partial discharge recognition using the cross wavelet transform in high voltage cable joint measuring systems using two opposite polarity sensors. Int J Electr Power Energy Syst May. 2020.;117(105695):1–8.
[11] Mor AR, Heredia LCC, Muñoz FA. A magnetic loop antenna for partial discharge measurements on GIS. Int J Electr Power Energy Syst Feb. 2020;115(105514):1–6.
[12] Mier C, et al. Magnetic and electric antennas calibration for partial discharge charge estimation in gas-insulated substations. Int J Electr Power Energy Syst Oct. 2022;141(108226):1–8.
[13] Ouyang Y, et al. A current sensor based on the giant magnetoresistance effect: design and potential smart grid applications. Sens Nov. 2012;12(11):15520–41.
[14] Mușuroi C, et al. High sensitivity differential giant magnetoresistance (GMR) based sensor for non-contacting DC/AC current measurement. Sens Jan. 2020;20(323):1–17.
[15] Li Y, Qian Z. The application of GMR sensor in the partial discharge detection. In: *2016 Int Conf Cond Monit Diagn (CMD)*, Xi'an, China; 2016. p. 924–7.
[16] Zhao G, et al. Tunneling magnetoresistive sensors for high-frequency corona discharge location. IEEE Trans Magn Jul. 2016;52(7):1–4.
[17] Chen Y, et al. Giant magneto-resistive (GMR) sensor for non-contacting partial discharge detection. IEEE Trans Instrum Meas 2023.
[18] Li Z, Dixon S. A closed-loop operation to improve GMR sensor accuracy. IEEE Sens J Aug. 2016;16(15):6003–7.
[19] Mor AR, Muñoz FA, Heredia LCC. A novel antenna for partial discharge measurements in GIS based on magnetic field detection. Sens Feb. 2019;19(4):1–17.
[20] PDflex. *Unconventional partial discharge analysis*. [Online]. Available: http://pdflex.tudelft.nl.
[21] Mor AR, Heredia LCC, Muñoz FA. A novel approach for partial discharge measurements on GIS using HFCT sensors. Sens Dec. 2018;18(12):1–12.

Yun Chen was born in Guangdong, China, in 1993. She received the B.S. degree from the South China Agricultural University, China, in 2016 and the M.S. degree from the South China University of Technology, China, in 2019. She is currently working toward a Ph.D. degree at the South China University of Technology, China, and is an academic guest at the High Voltage Technologies Group of the Delft University of Technology, the Netherlands. Her research interests include high-voltage technology and partial discharge testing of electric power equipment.

Luis Carlos Castro Heredia was born in Cali, Colombia, in 1986. He received the B.S. and Ph.D. degrees from the Universidad del Valle, Colombia, in 2009 and 2015, respectively. He worked as a researcher at the High Voltage Technologies Group of the Delft University of Technology, the Netherlands, from 2016 to 2022. He will become a Senior Analog Electronics Designer in Sioux Technologies, the Netherlands, in 2023. His research interests include high-voltage technology, partial discharge testing, analog electronics and sensor interfacing.

Johan J. Smit was born in Dordrecht, the Netherlands, in 1949. He received the M.S. degree from the University of Amsterdam, the Netherlands, in 1974, and the Ph.D. degree from the State University of Leiden, the Netherlands, in 1979. He became a full professor at the Delft University of Technology, the Netherlands, in 1995 and has served as emeritus since 2015. Earlier, he was employed at the Kamerlingh Onnes Laboratory in Leiden, at KEMA's engineering company from 1979 to 1999, on the supervisory board of the South Holland Power Grid from 1999 to 2004, and general chairman of the International Symposium on HV Engineering in 2003, and as CEO at the foundation KSANDR in the field of T&D Asset Management from 2003 to 2015. In CIGRE, the global International Council on Large Electric Systems, he chaired the International Study Committee D1 on Materials and Emerging Technologies from 1992 to 2004, and he convened the area Substation Management for SC B3 since 2005. His standardization activities include the national chairmanship of the board of the Royal Dutch Electrotechnical Committee (NEC-NL) since 2020, and the international chairmanship of IEC TC 112, Electrical Insulation Materials and Systems, since 2018. His research focuses on super/smart/sustainable high voltage solutions for power grids.

Mohamad Ghaffarian Niasar was born in Tehran, Iran, in 1984. He received the M.S. degree from the Sharif University of Technology, Iran, in 2008, and the Ph.D. degree from the Royal Institute of Technology, Sweden, in 2015. He is currently an assistant professor at the High Voltage Technologies Group of the Delft University of Technology, the Netherlands. His main research interests are the aging of electrical insulation, HVDC insulation system, partial discharges, high-frequency power transformers, power cables, and FEM modeling.

Robert Ross was born in Rotterdam, the Netherlands, in 1958. He received the M.S. and Ph.D. degrees from the Utrecht University, the Netherlands, in 1986 and 1990, respectively. He is a professor at the Delft University of Technology, the Netherlands, director of IWO (Institute for Science & Development), a professor at the HAN University, the Netherlands, and an Asset Management Research Strategist at TenneT (TSO in the Netherlands and part of Germany). At KEMA, he worked on reliability and post-failure forensic investigations. He was granted a SenterNovem Annual award and nominated Best Researcher by the World Technology Network for energy inventions. He was active in various committees in CIGRE, IEC, IEEE, and IEE. He recently wrote the Wiley/IEEE book "Reliability Analysis for Asset Management of Electric Power Grids" based on experience with utilities and the navy. His special fields of interest are reliable and sustainable energy supply and innovations like superconductivity and power electronics for the next generation grids.